Proc. of SPIE Vol. 1690, Design of Optical Instruments, ed. D M Aikens, V L Genberg, G C Krumweide, M J Thomas (Sep 1992) Copyright SPIE

Internal thermal emission analysis of an IR seeker

Daniel M. Brown

Teledyne Brown Engineering, Sensor Systems Department
Cummings Research Park, Huntsville, AL 35807

ABSTRACT

The focal plane of an infrared seeker was plagued with ghost images and nonuniform stray light irradiance. Teledyne Brown Engineering was tasked to determine the irradiance source and propose inexpensive solutions to the problems. First order analysis approximately modeled the focal plane irradiance and showed a serious flaw in the design. A design flaw allowed normal internally emitted thermal radiation to develop into a high level, nonuniform, focal plane irradiance. Exact ray tracing software, developed by the author, computed focal plane irradiance distributions which closely matched measured distributions. The software performs a non-sequential surface ray trace, splitting rays at partially reflecting surfaces (using a recursive algorithm), and computes internal thermal emission. The stray light problems could have been avoided in a design with the cold stop as the system aperture stop. This paper shows the method of analysis, results, and proposed solutions to the problem. This work demonstrates how infrared optical design requires special precautions and considerations. Methods and tools which work well in visible optical design may not work in infrared optical design.

1. INTRODUCTION

An infrared seeker was designed with an unconventional, uncooled, aperture stop. The apparent goal of this unconventional design was to enable the use of standard off-the-shelf dewar assemblies, rather than fabricate special dewars with correctly sized and positioned cold stops. Seeker prototype testing revealed the design suffered from two major problems which could not be explained by its developer. First, the design produced a ghost image on the focal plane opposite the target image. The developer attempted to solve this problem by turning off half the focal plane, reducing the field-of-view (FOV) by 50%, and biasing the center of the FOV to the center of one half of the focal plane. Second, a high level, nonuniform, background irradiance masked any reasonable target signal. Internal thermal emission was so severe that the irradiance difference with and without a cold-cap on the sensor was almost imperceptible. The developer attempted to solve this problem with an electronic high-pass filter.

Teledyne Brown Engineering (TBE) was tasked to determine the source of the ghost image and high level irradiance modulation on the focal plane and propose solutions which would restore the seeker to its original intended performance. Code V[1] was used to model the ghost image. First order analysis approximately modeled the focal plane irradiance and showed a serious flaw in the design. Exact ray tracing software, developed by the author, computed focal plane irradiance distributions which closely matched distributions measured by R. Crouse of TBE and D. Bradley of USASDC (see Acknowledgements). The software performs a non-sequential surface ray trace, splitting rays at partially reflecting surfaces (using a recursive algorithm), and computes focal plane irradiance due to internal thermal emission.

Analysis showed that the high level stray light problems could have been avoided in a design with the cold stop as the system aperture stop, ie. a 100% cold-stop efficiency. Cold-stop efficiency in the original design was 13%. The ghost image was due to a concave reflector at the aperture stop, used to image the cold shield onto the detector and reduce stray light. The author proposed an inexpensive solution (the TBE solution) which completely eliminates these problems and increases signal-to-noise by about 18.6 dB (computed from ray tracing). The solution consists of a minor redesign of the cold shield and dewar, and removal of the concave reflective baffle. The solution increases cold-stop efficiency to 100% and restores use of both halves of the focal plane array.

The method of analysis, proposed solutions to the problems, and results are discussed. Solutions proposed by others are also analyzed. None of these other solutions completely remove the stray light problems. Only the TBE solution simultaneously removes the ghost image and the high level, nonuniform focal plane irradiance.

2. ANALYSIS OF PROBLEM

The original seeker design violates common practice in military infrared design and produces expected results. Ghost imaging and high level background irradiance are the results of three major design flaws; 1) an unnecessary concave reflective baffle, 2) poor cold-stop efficiency, and 3) improper location of the bandpass filter. The result is a significantly reduced signal-to-noise ratio and reduced seeker acquisition range.

2.1 Ghost image analysis

The ghost image problem is illustrated in Fig. 1. The figure shows the primary image of a target about 1 mm left of center on the focal plane and its "half-moon" ghost image in the opposite quadrant. (The ghost image irradiance is less than a third of the primary image irradiance, but the gray scale was adjusted to enhance reproduction of the figure.) The two other streaks are believed to be bad pixels. The ghost image is a result of incorporating an uncooled concave reflective baffle as the system aperture stop, rather than the cold shield. The concave baffle images the detector back onto itself, albeit a defocused inverted image, to reduce stray light on the detector. (Note: conventional wisdom would have the baffle image the cold stop back onto itself.) Specularly reflected light from the target image on the detector is refocused by the concave reflector to the opposite quadrant on the focal plane, forming a blurred ghost image.

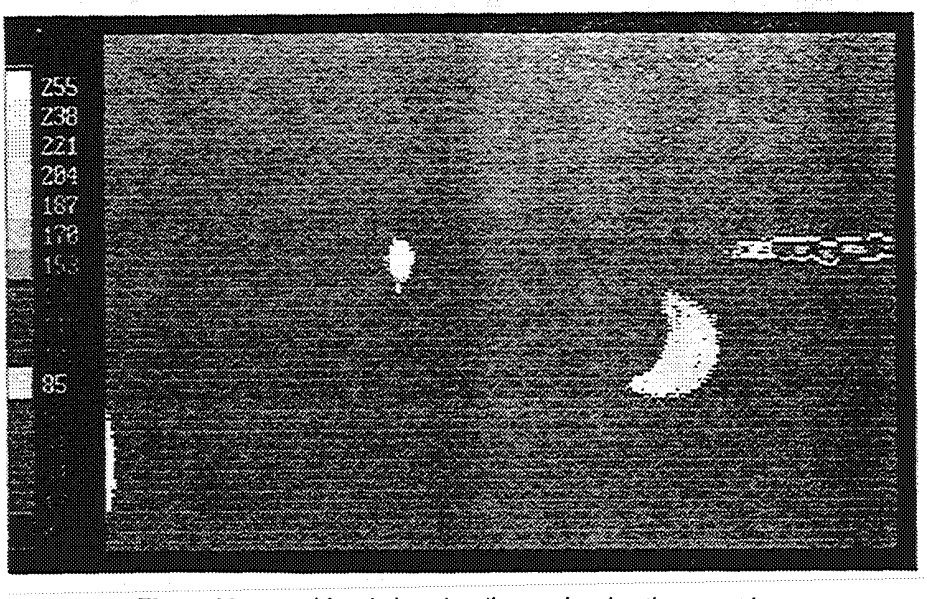

Fig.1 Measured focal plane irradiance showing the target image (just left of center) and its half-moon ghost image.

The ghost image was modeled in Code V to verify the stray light source. Fig. 2 shows a meridional fan of rays through the aperture stop focused to a point 1 mm off center on the detector. (Only the unobstructed rays are drawn.) Specularly reflected light from this point is reimaged by the baffle into the opposite quadrant. The secondary image point forms ahead of the detector, resulting in a circular blur spot on the detector. The aperture stop vignettes some of the reflected rays, resulting in the "half-moon" appearance of the blur spot.

The two-dimensional shape of the ghost-image can be predicted with spot diagrams from exact ray tracing. Fig. 3 shows spot diagrams of this ghost image for three different primary image positions. As the figure shows, the blur spot is clipped by the circular aperture stop at small field angles and clipped by the rectangular cold shield at large field angles.

The center spot diagram in Fig. 3 corresponds to the measured ghost image in Fig. 1. Agreement between the spot diagram and actual ghost image is excellent. Specular reflection off the focal plane properly accounts for the observed ghost image; diffuse scattering does not. Reflections off the window or cold stop also do not model the observed ghost image. It is apparent that eliminating the ghost image requires either: 1) eliminating specular reflection from the focal plane, 2)

significantly reducing the radius of curvature of the baffle, or 3) complete removal of the reflective baffle.

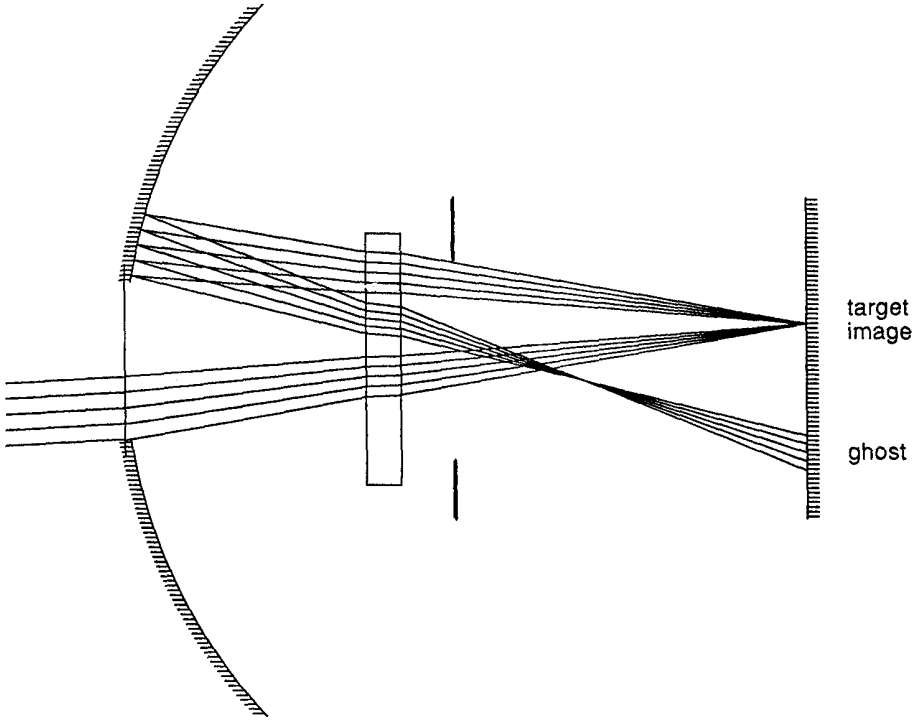

Fig. 2 Exact ray trace of ghost image formed by specularly reflected light from target image being reimaged by the concave baffle.

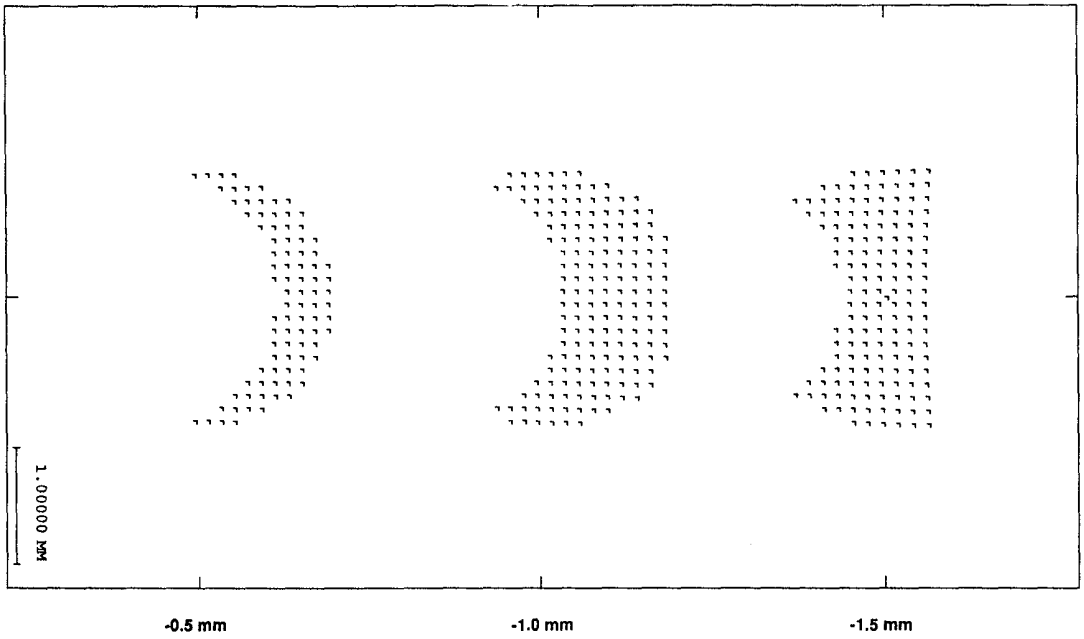

Fig. 3 Spot diagrams of ghost image as a function of primary image position on detector, determined by exact ray tracing. Half-moon shape agrees with actual measurements (see Fig. 1).

2.2 First order analysis of irradiance

The ratio of solid angles subtended (at the focal plane) by the (unobscured or clear) system aperture stop and the dewar cold shield, often called the "cold-stop efficiency," was about 13% in the original design. High performance military infrared sensors are generally designed with 100% cold-stop efficiency, ie. the cold stop is the aperture stop. Further, the cold stop (and aperture stop) should not be vignetted over the FOV of the system, otherwise the detector may be flooded with internally emitted thermal radiation. In the original design the cold stop is severely vignetted over the entire FOV, even on axis, as it is not used as the aperture stop. The detector receives stray light over the 0.35-steradian solid angle subtended by the rectangular cold stop but target signal light over only 0.046 steradians subtended by the aperture stop (hole in center of concave reflective baffle). Since intensity is proportional to the solid angle through which the light is received, the reduction in signal-to-noise ratio due to this less-than-optimal cold-stop efficiency is about 9 dB.

The location of the narrow band filter in the original design allows stray light over the entire blackbody spectrum to reach the detector. The integral of the effective spectral response of the detector (product of blackbody and quantum efficiency spectrums) within the pass band of the filter is only about 16 percent of the integral over the entire spectrum, as illustrated in Fig. 4. The cost of locating the filter remote from the dewar window, allowing out-of-band stray radiation to reach the detector, is a further reduction of signal-to-noise by about 8 dB.

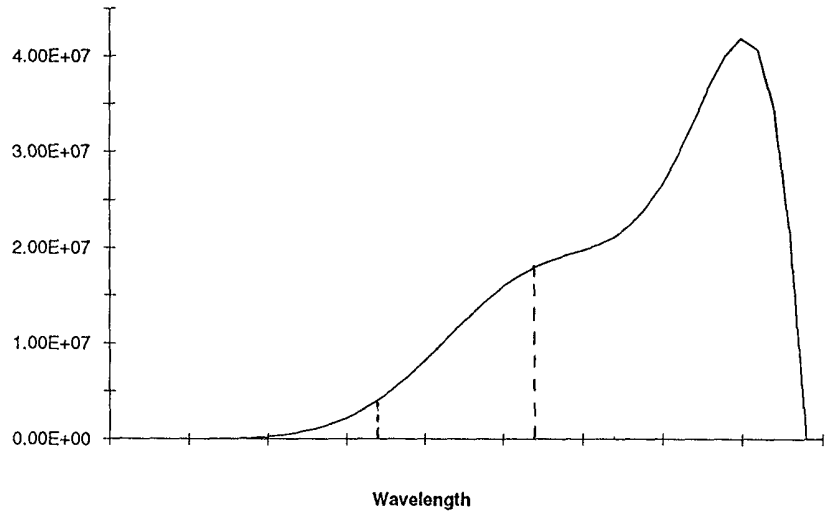

Fig. 4 Product of focal plane responsivity and blackbody spectrums (at certain temperature). Out-of-band flux reaching detector can cause significant reduction of signal-to-noise ratio. (Scale values intentionally omitted.)

In accordance with good detector design, the interior side of the cold stop (facing the detector) is a high emissivity blackened surface. The exterior side of the cold stop is gold coated to minimize heat transfer from warm elements. However, the concave reflective baffle produces an image of the reflective cold stop onto the detector. Although the cold stop itself has low emissivity, it reflects stray light from other elements (e.g. window and concave baffle) in all directions. Thus the reflective cold stop is effectively a radiant emitter.

Fig. 5 shows a first order (paraxial) ray trace for imaging the lower edge of the cold stop onto the detector. The upper and lower rim rays in the figure (the sum and difference of the chief and marginal ray heights) show the upper and lower extent (to first order) of the blur spot on the detector. This ray trace shows that a blurred image of the cold stop is superimposed onto the detector. We would expect from first order analysis alone to find a detector irradiance distribution which is high toward the edge and which has a dark rectangular central region with dimensions proportional to the cold stop. This is in fact what was observed in the laboratory. Fig. 6 shows the irradiance distribution measured in the laboratory (by Crouse and Bradley) with the high-pass electronic filter turned off. In agreement with the first order ray trace, the irradiance is low in the center and increases toward the edges. A blurred image of the rectangular cold stop is clearly visible. Imaging the cold stop onto itself,

rather than onto the focal plane would have given a flat irradiance distribution; however, the cold-stop efficiency would remain low.

	0	1	2	3	4	5	STO	7
$-\phi$	0	0	0	-.13333	0	0	0	0
t/n	1.5	.2914	6.83502	6.83502	.2914	1.5	10.0	
y	0	.5525	.6598	3.1772	2.7991	2.7830	2.7000	2.1468
nu	.3683	.3683	.3683	-.0553	-.0553	-.0553	-.0553	
$\bar{y}$	-2.7	-2.783	-2.7991	-3.1772	-.6598	-.5525	0	3.6832
$n\bar{u}$	-.0553	-.0553	-.0553	.3683	.3683	.3683	.3683	

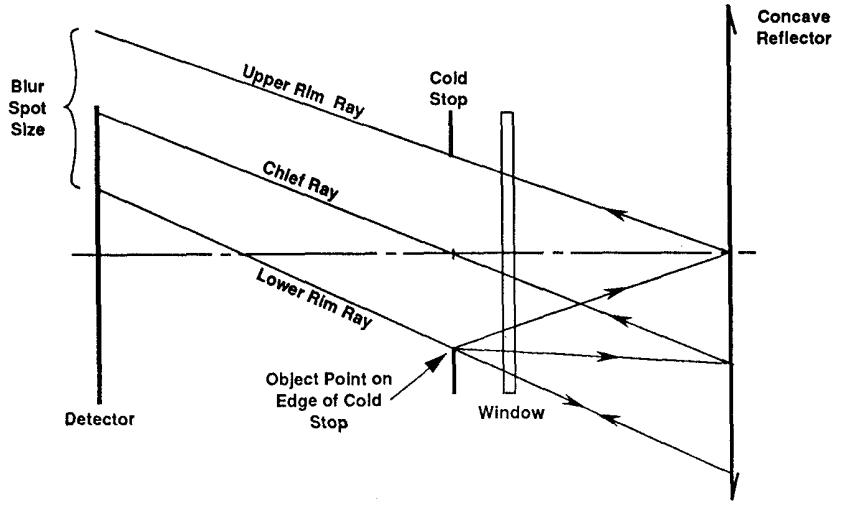

Fig. 5 First order ray trace of the cold stop imaged onto the detector by the concave baffle.

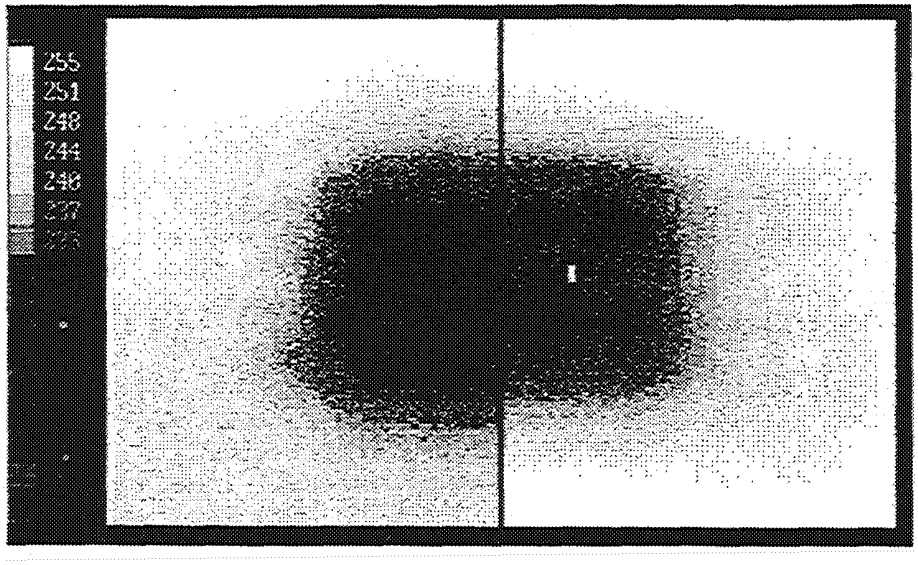

Fig. 6 Measured background focal plane irradiance (cold cap on lens) without high-pass electronic filter.

Numerical calculations of the thermal radiation emitted directly from the dewar window and reflective baffle agree with the minimum irradiance on the detector, measured on axis. Multiple reflections account for the irradiance increase toward the edges of the focal plane. Multiple reflections between the cold stop, dewar window, concave baffle, and filter allow the detector to "see" a considerable amount of radiance from sensor package walls and lens mounts. These multiple reflections superimpose a blurred image of the cold stop and baffle onto the detector. Exact ray tracing is required to accurately model the irradiance modulation.

Clearly, the combination of reflective cold stop and reflective baffle is a fatal system design flaw. It is noted that the supplier of the detector / dewar is a competent sensor system designer and would unlikely have made this mistake. However, the seeker developer kept the detector supplier unaware of the application and thus was not able to benefit from the supplier's experience.

2.3 Exact ray trace analysis of irradiance

Exact ray tracing was the primary method used to compute focal plane irradiance from internal thermal emission. Rays are traced from points on the detector through a grid of points in the aperture of the cold shield and through multiple reflections between all element surfaces. Absorptance along each ray path is computed. Assuming thermal equilibrium, such that the directional emissivity equals the absorptivity in the opposite direction,

$$\varepsilon(\vec{r}) = \alpha(-\vec{r}), \tag{1}$$

the irradiance at each point on the detector can be computed.

Figure 7 shows part of the original layout of the system and illustrates this ray trace method. The figure shows the unobscured meridional fan of rays traced from a single detector point, through the rectangular aperture of the cold shield, through the dewar window, reflected off the concave baffle, and terminating on the exterior surface of the cold shield (for clarity, rather than reflecting off the cold shield). The hole in the center of the baffle is the system aperture stop. Refractive elements to the right of the aperture stop are not shown. Clearly, the radiant flux incident on the detector within a solid angle increment about each ray is due to four contributions; 1) direct emission from the window, 2) emission from the concave baffle reduced by the window transmittance, 3) emission from the window reduced by one reflection from baffle and one transmission through window, and 4) emission from the window reduced by a reflection from the cold shield, reflection from the baffle, and two transmissions through the window. It is also apparent that continuing the ray trace through multiple reflections between the surfaces (cold shield, two window surfaces, baffle, and elements to the right of baffle) would provide additional flux contributions.

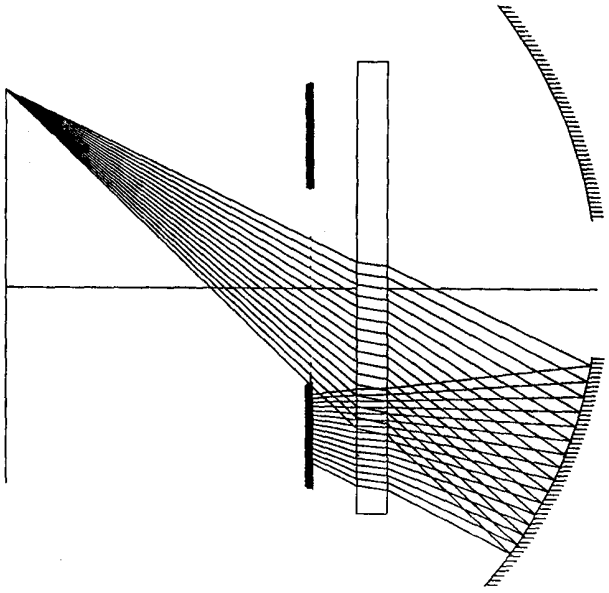

Fig. 7 Thermal radiation reflected off dewar cold shield and imaged onto detector by reflective baffle.

Software was developed to trace exact rays through multiple reflections between element surfaces and compute the absorptance along each ray path. It was necessary to develop an algorithm which handled partial reflectance because the narrow band filter in the original design (located to the right of the baffle in Fig. 7) allowed out-of-band thermal radiation incident on the dewar window to reach the detector. The dewar window is anti-reflection (AR) coated for in-band radiation but becomes increasingly reflective above band where a significant portion of blackbody radiation occurs (Fig. 4). The reflectivity of the window varies from 1 to 15 percent in this region. Thus, the ray trace code had to be able to account for partial reflectance and transmittance at the dewar window and narrow band filter.

A recursive ray trace procedure (one that calls itself) was implemented to handle partial reflectance. At every partially reflecting surface the ray is split into a reflected ray and refracted ray. The reflected ray path is followed first until ray failure or total absorption, then the refracted ray path is followed. Absorptances for the two paths are combined. Figure 8 shows the algorithm for this procedure.

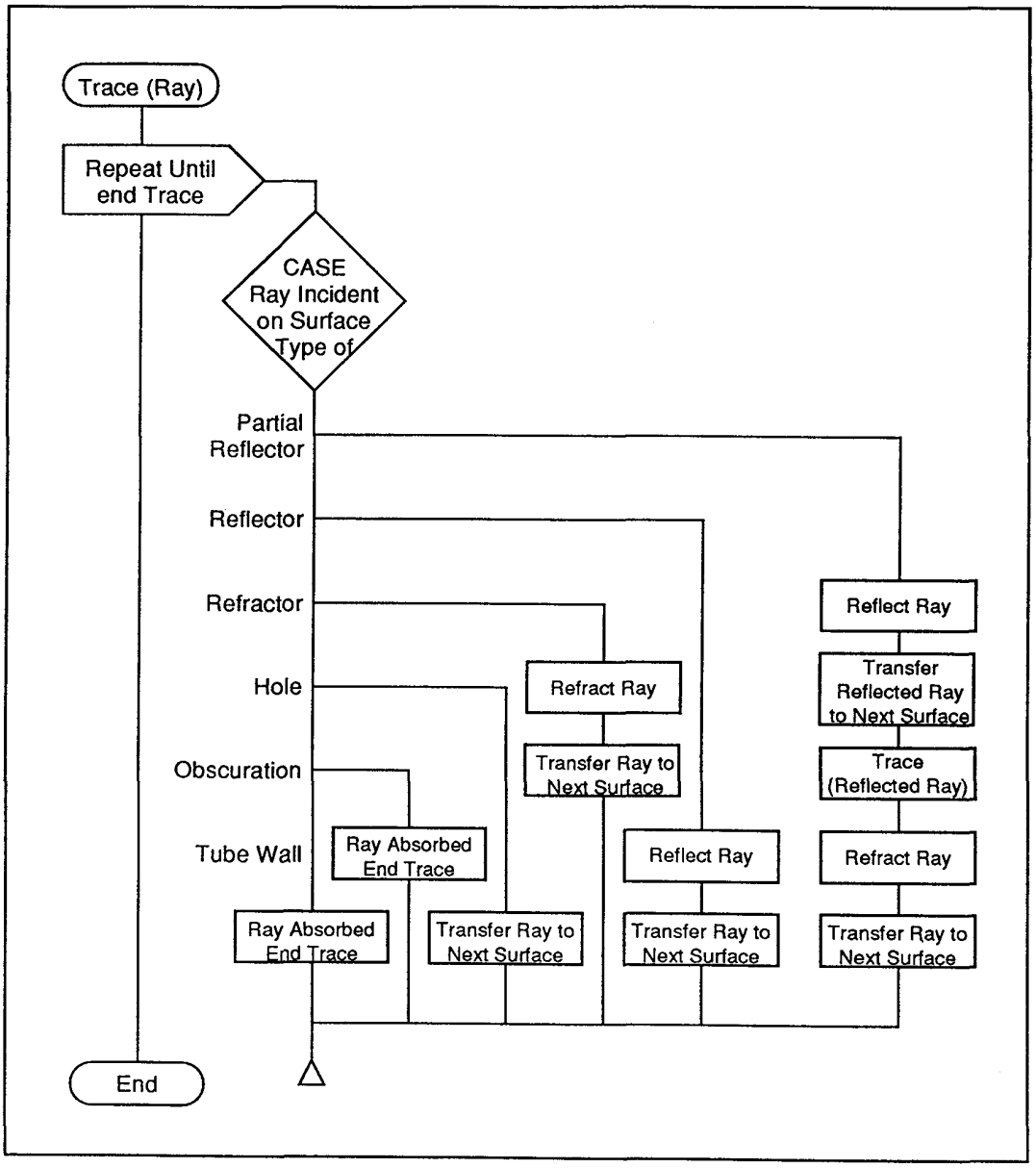

Fig. 8 Recursive ray trace procedure for handling partially reflecting surfaces

The lens system is entered via standard surface parameters such as; surface curvature, thickness, refractive index, and type of surface using a global coordinate system. Each surface is also assigned dimensions for clear aperture (either rectangular or circular). Values for reflectivity, absorptivity, and transmissivity obtained from the literature[2-5] are assigned to each surface.

These last three parameters should not be confused with reflectance, absorptance, and transmittance which take into account multiple reflections between two or more surfaces. Reflectivity quantizes a single surface reflection and equals reflectance only for infinitely thick slabs or opaque surfaces. Absorptivity and transmissivity are normally redundant parameters related by

$$\alpha = 1 - \tau \tag{2}$$

and quantize the absorption properties of the media to the right of each surface. Absorptivity and transmissivity do not include losses due to surface reflection, but are entered as independent parameters to also model scattering and non-thermal equilibrium surfaces such as those inside or on the dewar. To distinguish between these six radiation parameters and illustrate the calculations performed by the code, consider the thick (non-interfering) transparent slab illustrated in Fig. 9 with two different surface reflectivities, ρ_1 and ρ_2. Equation (2) is assumed for the absorptivity, α, and transmissivity, τ, of the dielectric media between the two surfaces. A ray of unit intensity is incident on the first surface from the left. The reflectance, R, is the geometric series sum of all the contributions reflected to the left and is given by

$$R = \rho_1 + \frac{(1-\rho_1)^2 \tau^2 \rho_2}{1 - \tau^2 \rho_1 \rho_2} \tag{3}$$

The transmittance, T, is the sum of the contributions transmitted to the right.

$$T = \frac{\tau (1-\rho_1)(1-\rho_2)}{1 - \tau^2 \rho_1 \rho_2} \tag{4}$$

Likewise, the absorptance is given by

$$A = \frac{(1-\rho_1)(1+\tau\rho_2)\alpha}{1 - \tau^2 \rho_1 \rho_2} \tag{5}$$

When $\rho_1 = \rho_2$ and Eq. (2) is assumed, these three radiation parameters reduce to the familiar forms;

$$R = \rho + \frac{(1-\rho)^2 \rho \tau^2}{1 - \rho^2 \tau^2} , \tag{6}$$

$$T = \frac{(1-\rho)^2 \tau}{1 - \rho^2 \tau^2} , \tag{7}$$

$$A = \frac{(1-\rho)(1-\tau)}{1 - \rho\tau} . \tag{8}$$

It is interesting that in the general case of unequal reflectivities, transmittance does not depend on which surface has higher reflectivity, whereas reflectance and absorptance do. This fact is important in determining how to position a narrow band interference filter. Equation (5) shows that the high reflectivity surface (surface with the dielectric stack) of an interference

filter should be positioned toward the detector to reduce out-of-band emittance toward the detector from the substrate.

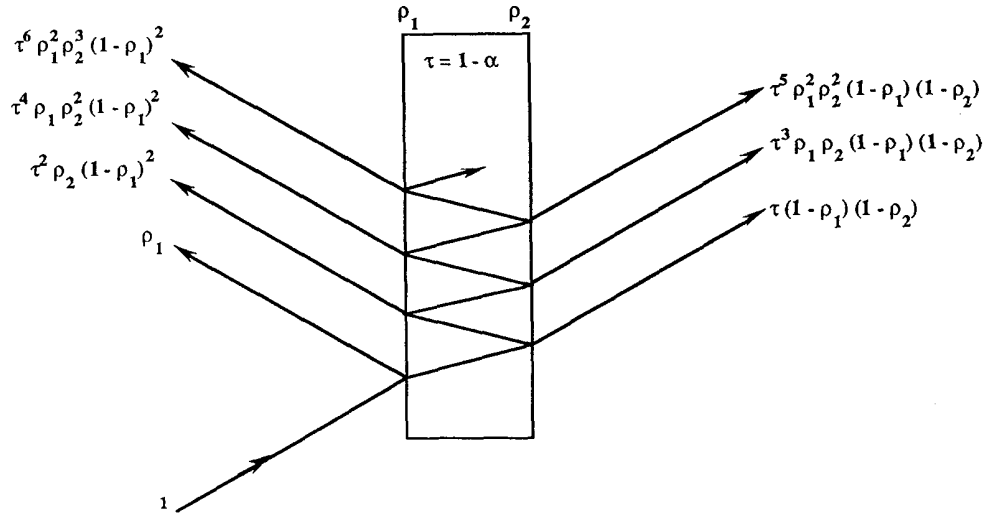

Fig. 9 Reflectance, transmittance, and absorptance due to multiple reflections between two surfaces with reflectivities ρ_1 and ρ_2 on a slab with absorptivity α, or transmissivity τ

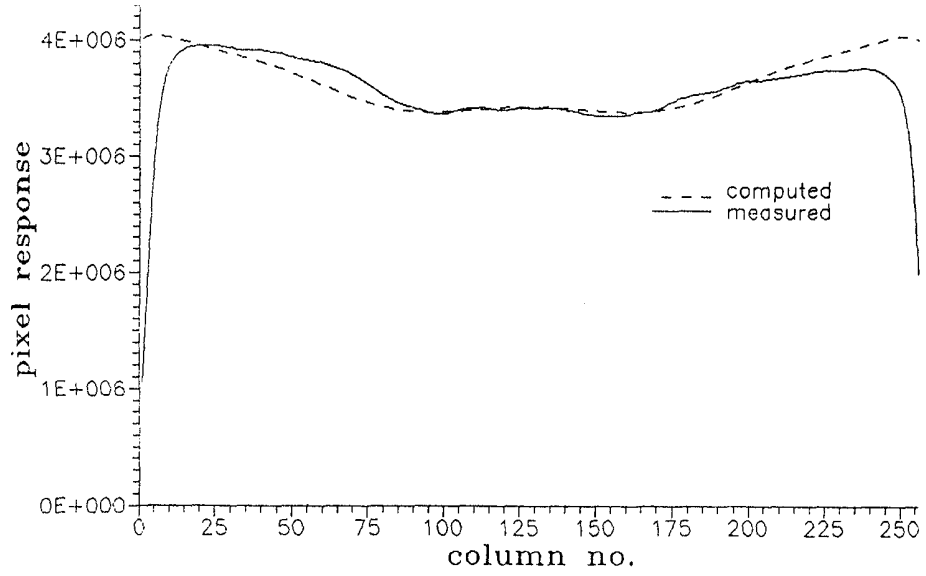

Fig. 10 Comparison of computed and measured focal plane irradiance distributions in horizontal direction across center of detector. Computed irradiance obtained by exact ray tracing.

The polished concave baffle in the original design has a high reflectivity and small emissivity. Both surfaces of the dewar window have low nonzero reflectivities with a low emissivity material between. The first surface of the bandpass filter in the system aperture stop has a high reflectivity out of band and low reflectivity in band. The thin film interference stack of the filter is assumed to be on the surface towards the detector, thus providing a low emissivity out of band. The cold stop is gold coated on the surface away from the detector to reduce heat transfer to the cold stop. For stray light calculations the cold stop was assumed to have zero emissivity. Effective reflectivities for the window and filter were obtained by integrating and normalizing the product of spectral reflectivity, spectral responsivity of the detector, and blackbody spectrum. For stray light predictions, effective reflectivities for the dewar window and filter were calculated to be 6 percent and 84 percent respectively.

The two-dimensional irradiance distribution of Fig. 6 was duplicated with our ray trace code. Fig. 10 shows the computed irradiance distribution across the center of the detector, along with the measured distribution for comparison. Having obtained excellent agreement between measurements and theory, we could proceed to evaluate solutions to the problem.

3. PROPOSED SOLUTIONS

The author's proposed solution to the problem consists of complete removal of the baffle, repositioning and resizing the cold stop, and relocating the bandpass filter in place of the dewar window. Specifically, the dewar cold stop should be made circular and shifted forward, away from the detector, by 8 mm and resized to 4.4 mm diameter, increasing cold stop efficiency to 100%. The dewar window is also moved forward by 8 mm. The original dewar window should be removed and replaced with the narrow band filter with the high reflectivity interference layer facing toward the detector. The filter should not be a sandwiched type, but one with the thin film layer on the surface of the substrate. Figures 11, 12, and 13 show the predicted detector irradiance with this modification. This solution provides the greatest reduction of stray light of all proposed modifications. This is the only modification which simultaneously eliminates irradiance modulation, reduces stray light, increases cold stop efficiency, and eliminates the ghost image problem. Reducing the radius of curvature of the reflective baffle would also reduce the ghost image and irradiance modulation, but does not improve cold-stop efficiency.

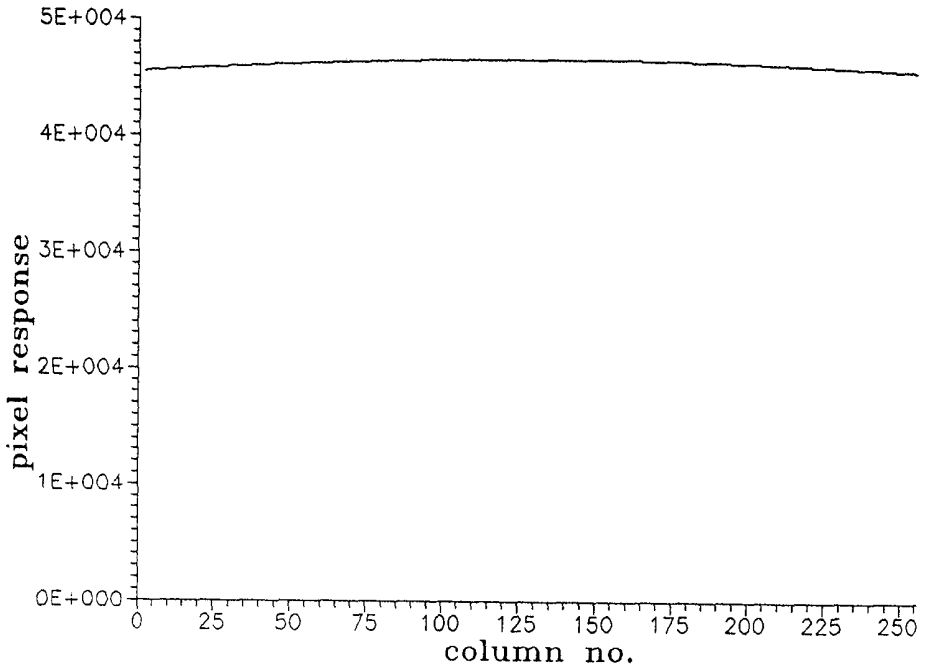

Fig. 11 Computed irradiance distribution for TBE's solution.

Subsequent to analysis and proposal of a solution, the developer requested evaluation of several alternative design modifications. Detector irradiances for these modified designs were computed and are shown in Figures 12 and 13. The same surface radiation parameters used to model irradiance for the original design were used to compute expected irradiances for the modified designs, except for the bandpass filter and dewar window. When the bandpass filter is located on the dewar, only blackbody radiation within the pass band reaches the detector. Its effective reflectivity and transmissivity are thus changed to 0.085 and 0.915 respectively. Effective reflectivity and transmissivity of the dewar window changes only slightly with relocation of the filter. The normalizing irradiance of a blackbody at the cold stop is also appropriately reduced.

One proposed modification relocates the bandpass filter onto the cold stop. The baffle would remain in the system. Figures 12 and 13 show the computed detector irradiance with this design modification. The overall level of stray light has been reduced but the percent modulation has increased slightly. This is due to the fact that out-of-band direct emission from the window has been eliminated, but the multiple reflections have not. Contributions due to multiple reflections, relative to direct emission, are thus increased. This proposed modification does not eliminate the ghost image problem or increase cold

stop efficiency.

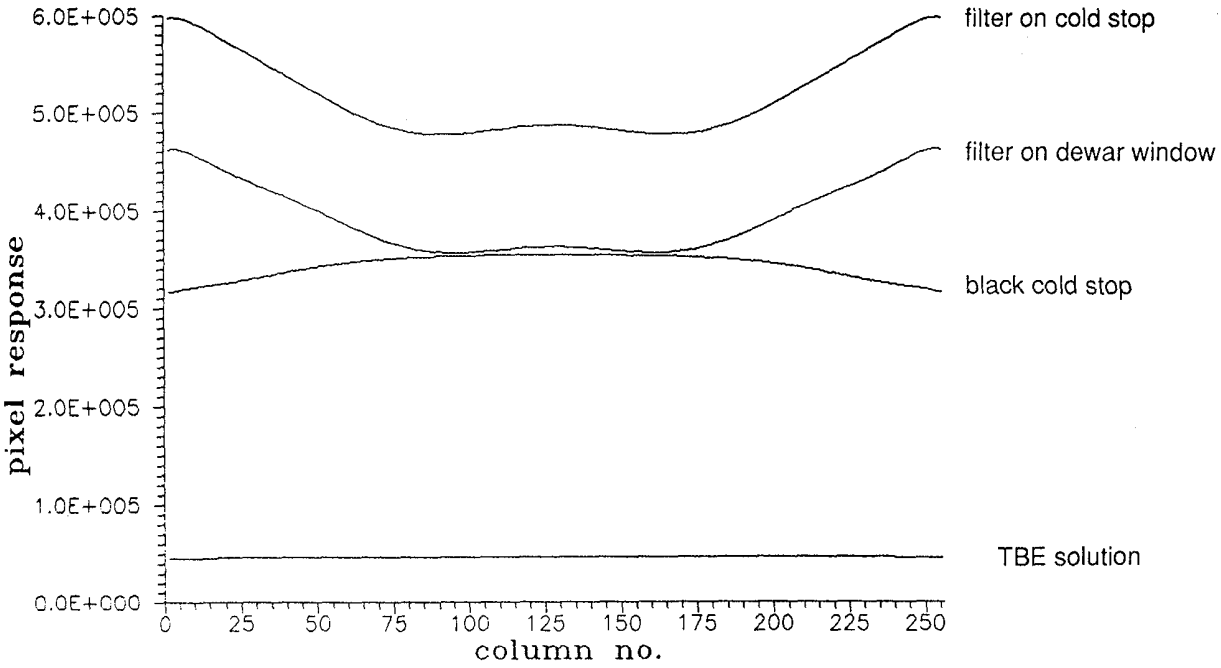

Fig. 12 Computed irradiance distributions for four different proposed design modifications.

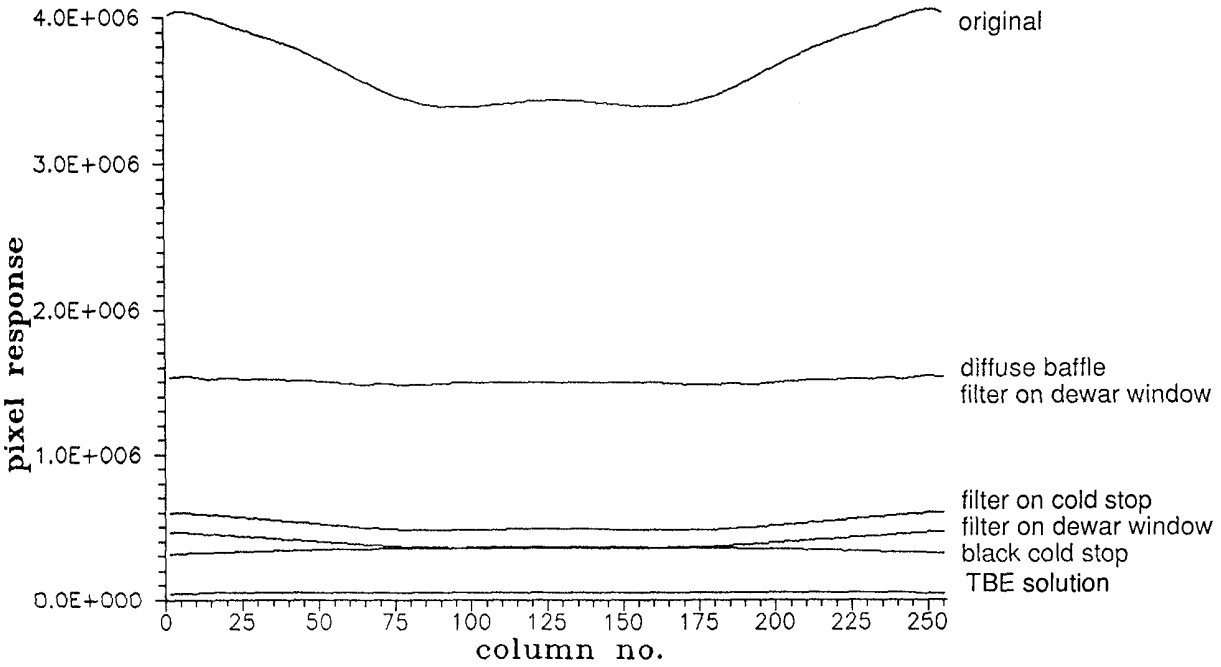

Fig. 13 Computed irradiance distributions for original design and five different proposed design modifications. Level for diffuse baffle without filter relocation would be significantly higher than original design.

A second proposed design modification locates the filter on or in place of the dewar window but leaves the baffle in place. Assuming the interference coating is located toward the detector, the finite emissivity of the warm filter will still be insignificant. Figures 12 and 13 show the computed detector irradiance with this modification. As with the above design modification, multiple reflections are not eliminated, only the out-of-band radiation. The irradiance is slightly lower than that

with the filter on the cold shield, apparently due to the reduction in mass of window material and number of partially reflecting surfaces. This modification does not eliminate the ghost image problem or increase cold stop efficiency.

A third proposed design modification locates the filter in place of the dewar window and makes the reflective cold stop a blackbody absorber. Reflections between baffle and cold stop are eliminated, but reflections between baffle and window are not. Figures 12 and 13 show the predicted detector irradiance. The increased heat transfer to the cold stop due to making it a blackbody absorber will affect cool-down time and should be quantized before adopting this solution. This modification significantly reduces irradiance modulation; however, it does not eliminate the ghost image problem or increase cold stop efficiency.

A fourth proposed modification locates the filter in place of the dewar window and makes the baffle a diffuse reflector. Increasing the surface roughness of the baffle will also increase its emissivity. The Infrared Handbook[5] gives a value of 0.21 for the emissivity of sandblasted aluminum. Reflected flux from a diffuse surface is composed of both specular and diffuse components. A significant portion of the diffuse component is absorbed by the sensor walls. Thus the effective emissivity of sandblasted aluminum is higher than 0.21. Fig. 13 shows the predicted detector irradiance with 0.30 and 0.70 for baffle emissivity and reflectivity with the bandpass filter on the dewar window. Although the modulation is removed, the irradiance is significantly higher than that of the other proposed designs which also locate the filter on the dewar. If the filter were not relocated, this modification would saturate the detector with stray light levels significantly higher than original design levels. Ghost imaging and low cold stop efficiency remain.

4. CONCLUSION

The author has shown a simple physical explanation for the irradiance modulation and ghost image on the detector. Both exact ray tracing and first order theory produce results consistent with actual measurements. Several alternative design modifications were evaluated. Of these proposed solutions, only the TBE solution simultaneously reduces stray light, increases cold stop efficiency, and eliminates the ghost image, thus allowing the full potential of the infrared sensor to be realized.

Repositioning the cold stop and repositioning the narrow band filter both reduce stray light incident on the detector and thus increase the signal-to-noise ratio. Resizing and repositioning the cold stop reduces the solid angle through which stray light is incident from 0.3456 steradians to 0.0469 steradians. With the filter on the dewar window only in-band stray radiation can reach the detector, which is about 16 percent of that originally reaching the detector. These modifications together reduce stray light noise by 16.6 dB (not including the effects of eliminating multiple reflections). Exact ray tracing computed the stray light reduction to be 18.6 dB, or to a level about one percent of its original level. Additionally, the background detector irradiance will be significantly flattened due to the absence of multiple reflections from the baffle. The only modulation will be a slight decrease of irradiance toward the edge due to the decrease of the projected area of the window with the cosine of the angle. The edge of the detector will see an irradiance level which is 98% of that on axis. This modulation is insignificant and the ghost image is completely eliminated.

A clear definition of cold-stop efficiency appears to be needed among the infrared sensor community. Indeed, this author has evaluated reimaging cassegrain designs with significant central obscurations which were advertised to have 100% cold-stop efficiency! Placing the cold stop at the aperture stop position (or its image) is a necessary condition for 100% cold-stop efficiency; but in this author's opinion, it is not a sufficient condition. The clear aperture of the cold stop must also be unvignetted and unobscured. A definition for cold-stop efficiency which accounts for obscuration would be, "the ratio of the solid angle at the detector through which the signal is incident, to the solid angle subtended by the cold stop." Thus, cold-stop efficiency is important under low levels of external background radiation: when internal thermal emission becomes significant compared to external thermal sources.

This study demonstrates the importance of thorough analysis and critical design review, especially when seeker designs take an unconventional approach. It is noted some of the issues discussed in this paper are not a concern in visible spectrum optical design. Designers can not approach infrared design with only the tools used for visible design. Analysis of stray light, from both external and internal sources, becomes necessary in infrared seeker design.

Notwithstanding security issues, the probability of occurrence of problems like this can be minimized if the prime

contractor accepts his subcontractors as "team players" on the project, especially when a subcontractor is more knowledgeable in a certain area than the prime. A subcontractor often has just as much interest in seeing the project become a success as the prime and will often give free advice if invited to do so as a member of the team.

5. ACKNOWLEDGEMENTS

The Joint Theater Missile Defense Program Office of the USA Strategic Defense Command (USASDC) provided funding for this work. The author wishes to thank Randy Crouse of TBE and Daniel J. Bradley of USASDC for measuring the focal plane irradiance on the sensor and initiating the research to determine the source of the problems.

6. REFERENCES

1. Commercial lens design program available from Optical Research Associates, Pasadena, CA.

2. Manufacturers catalog data for germanium and silicon optics, Eagle Picher Electro-Optic Materials, Quapaw, OK 74363.

3. Y.S. Touloukian and D.P. DeWitt, Thermophysical Properties of Matter, Vols. 7 and 8, Plenum, N.Y. (1972).

4. Y.S. Touloukian and C.Y. Ho, Thermophysical Properties of Selected Aerospace Materials, Purdue Research Foundation, West Lafayette, Indiana (1976).

5. W.L. Wolfe and G.J. Zissis, The Infrared Handbook, Environmental Research Institute of Michigan, (1989).